Determination of Causative Fault Parameters for the October 17, 2009, Ray-Tehran Earthquake, Using Near Field SH-Wave Data

H. Hamzehloo[1], F. Sinaeian[2], M. Mahood[3], H. Mirzaei Alavijeh[4], and E. Farzanegan[4]

1. Associate Professor, Seismology Research Center, International Institute of Earthquake Engineering and Seismology (IIEES), Tehran, I.R. Iran, *Corresponding Author; email: hhamzehloo@iiees.ac.ir
2. Assistant Professor, Building and Housing Research Center, Tehran, I.R. Iran
3. Ph.D Graduate, Seismology Research Center, International Institute of Earthquake Engineering and Seismology (IIEES), Tehran, I.R. Iran
4. Research Associate, Building and Housing Research Center, Tehran, I.R. Iran

ABSTRACT

In this paper, the strong motion accelerograms of October 17, 2009, Tehran-Ray earthquake ($M_w = 4.0$) of south of Tehran were analyzed. (i) Using derived SH-wave spectral data, at first the parameters W_o (long period spectral level), f_c (corner frequency) and Q(f) (frequency dependent, average shear wave quality factor), appropriate for the best-fit Brune ω^{-2} spectrum of this event were estimated. Then a non-linear least square analysis of the SH-wave spectral data was performed to provide objectively approximate near field estimates of the strike, dip and rake of the causative fault. Based on this analysis, the first fault plane solution has been presented for this event, which may be related to Eyvanaki fault closed to Tehran. Near field estimates of the strike, dip and rake of the causative fault of the 2009 Ray-Tehran earthquake are 292°, 36°, and 59°, respectively. Our estimated fault plane solutions suggest a reverse faulting mechanism with minor left lateral strike slip component. The estimated strike is consistent with the direction of isoacceleration map and Eyvanaki fault.

Keywords:
The 2009 Ray-Tehran earthquake;
Near field;
Causative fault

1. Introduction

Tehran, the capital city of Iran, is located in a very high seismic zone at the foot of the Alborz Mountains. The Alborz is seismically active with *E-W* trending mountain belt of 100*km* wide and 600*km* long, which was formed in the late Triassic [1]. The recent Cenozoic evolution has been explained as the result of strain partitioning between left-lateral strike slip and thrust faults parallel to the belt [2-3]. North-south shortening of 8±2*mm/yr* has been reported across Alborz range between the central Iran and the Southern Caspian shore [4]. Its total shortening is estimated to be 30*km* at the longitude of Tehran since the early Pliocene [3]. The Central Alborz has an arcuate shape toward central Iran and Tehran is situated near its maximum curvature on the southern flank [5]. Several active faults affect the city, see Figure (1). To the north, the Khazar and North Alborz reverse faults dip southward with a slight component of left lateral strike slip motion [3]. Bounding the highest topography to the south, the main active faults are the North Tehran and Mosha faults and their westward continuation, the Taleghan fault [3, 6, 7]. The Mosha fault has accommodated a total left lateral displacement of 30-35*km* and the present day average rate is of 3*mm/yr* [8-9]. To the south of Tehran, the Ipak, Eyvanaki, Garmsar and Pishva Faults, see Figures (1) and (2), also exhibit mostly oblique reverse left lateral motion [7, 10].

The distribution of historical earthquakes around Tehran, see Figure (1), shows that the region has been experiencing eight large destructive earthquakes with magnitude greater than 7 from 4^{th} *B.C* to 1830 [11]. These large historical earthquakes caused severe damage to Shahre Ray city, which is a part of Tehran city at present. The last large

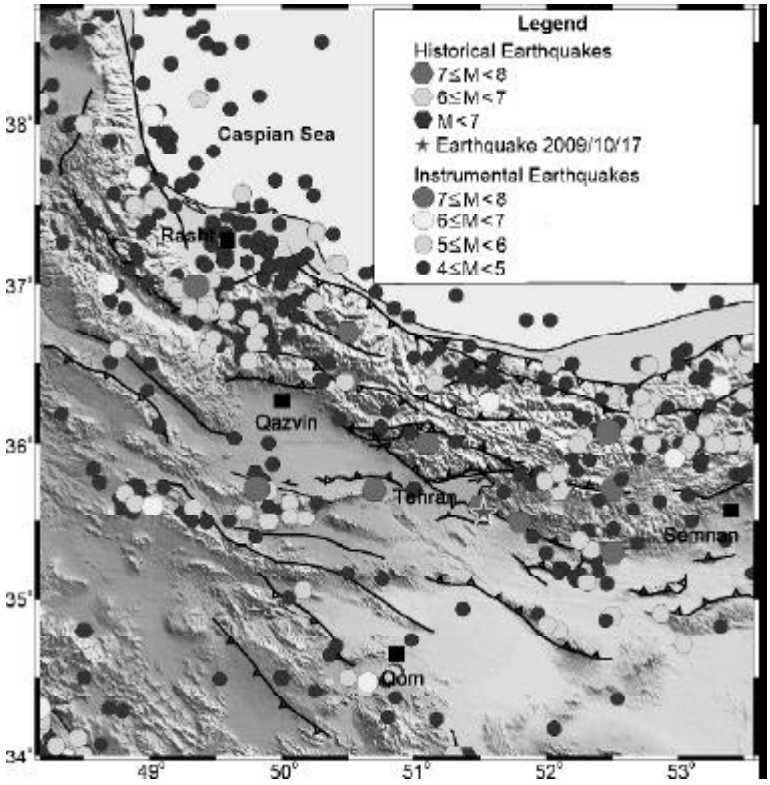

Figure 1. Active faults and seismicity around Tehran.

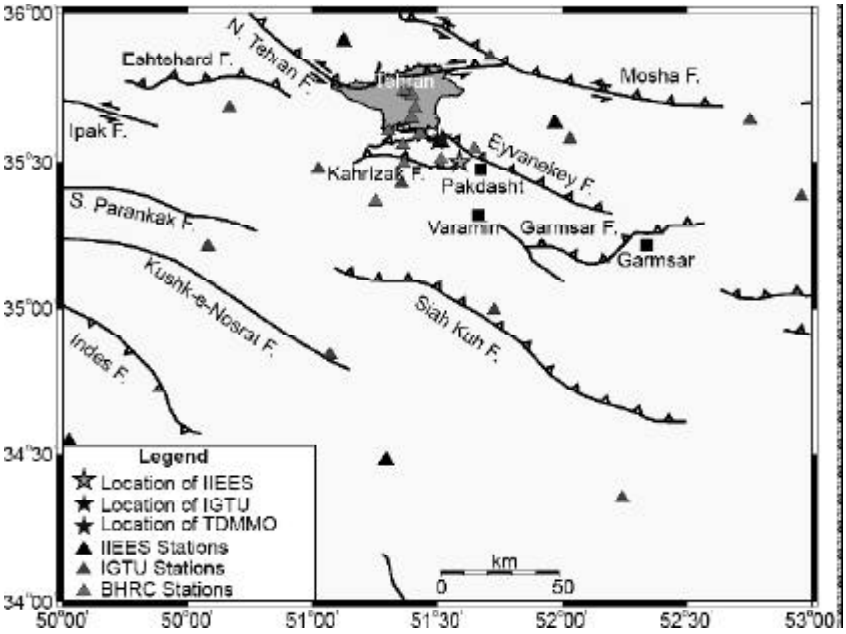

Figure 2. The locations of epicenter reported by IIEES, IGTU and TDMMO.

historical event was the 1830 earthquake with magnitude 7.1, which occurred approximately 100*km* from the city. The closest historical event in the city was the 855 earthquake with magnitude 7.1 [12]. The most important instrumental earthquakes, which occurred in this region, are the 1962 Buin Zahra earthquake with magnitude $M_W = 7.2$, the 2002 Changureh (Avaj) earthquake with magnitude $M_W =$ 6.5, and the 2004 Firozabad Kojor earthquake with magnitude $M_W = 6.3$ [12]. The strong ground motion network in Tehran recorded four large to strong earthquakes from 1990 to 2007. These records are related to the 1990 Manjil-Rudbar earthquake with magnitude $M_W = 7.3$, the 2002 Changureh (Avaj) earthquake with magnitude $M_W = 6.5$, the 2004 Firozabad Kojor earthquake with magnitude $M_W = 6.3$

and the 2007 Kahak-Qom earthquake with magnitude M_W= 5.9.

Recently, the earthquake with magnitude M_W = 4.0 occurred at 14:23:57 local time on October 17, 2009 in south of Tehran, see Figures (1) and (2). This earthquake was felt at Tehran. Since Tehran is located in a very high seismic zone, it is therefore important to study this earthquake in more detail in order to identify the causative fault parameters. For this purpose, the causative fault parameters were estimated by using *SH*-waves analysis of recorded acceleration data.

2. The 2009 Ray-Tehran Earthquake

On October 17, 2009, at 14:23:57 (local time), an earthquake, with estimated magnitude M_W = 4.0, occurred in the southeastern of Tehran. The earthquake was felt not very strongly in Tehran. Various agencies e.g. International Institute of Earthquake Engineering and Seismology (*IIEES*), Institute of Geophysics, Tehran University (*IGTU*), and Tehran Disaster Mitigation and Management Organization (*TDMMO*) [13] estimated the hypocentral locations of this event, see Table (1). The earthquake epicenter is located close to the Eyvanaki fault southeastern of Tehran, see Figure (2) with the local geological structures trending *NW-SE*.

Table 1. Hypocentral location reported by different agencies.

Lat. °N	Lon. °E	Depth (km)	Ref.
35.50	51.59	18	IIEES
35.57	51.50	12	IGTU
35.547	51.526	16.8	TDMMO

3. Strong Ground Motion Data

The 2009 earthquake was recorded by 12 *SSA*-2 type accelerographs of the strong motion array operated by *BHRC*, see Figure (2). In this study we reported a detailed analysis of this strong ground motion data recorded at Chehel Ghez (*CHE*), Ghaniabad (*QAN*), Ghaleno (*GHA*), Tehran-1 (*TE*1), Tehran-18 (*T*18), Hassan Abad (*HAS*), Tehran-2 (*TE*2), Tehran-29 (*T*29), Kahrizak (*KAH*), Tehran-13 (*T*13), Tehran-58 (*T*58) and Chahardangeh (*CHE*) stations, see Figure (2) and Table (1). The isoacceleration maps for two horizontal components and vertical component show approximately a *NW-SE* direction for causative fault, see Figure (3). These maps have been drawn to have an estimation of causative fault strike direction.

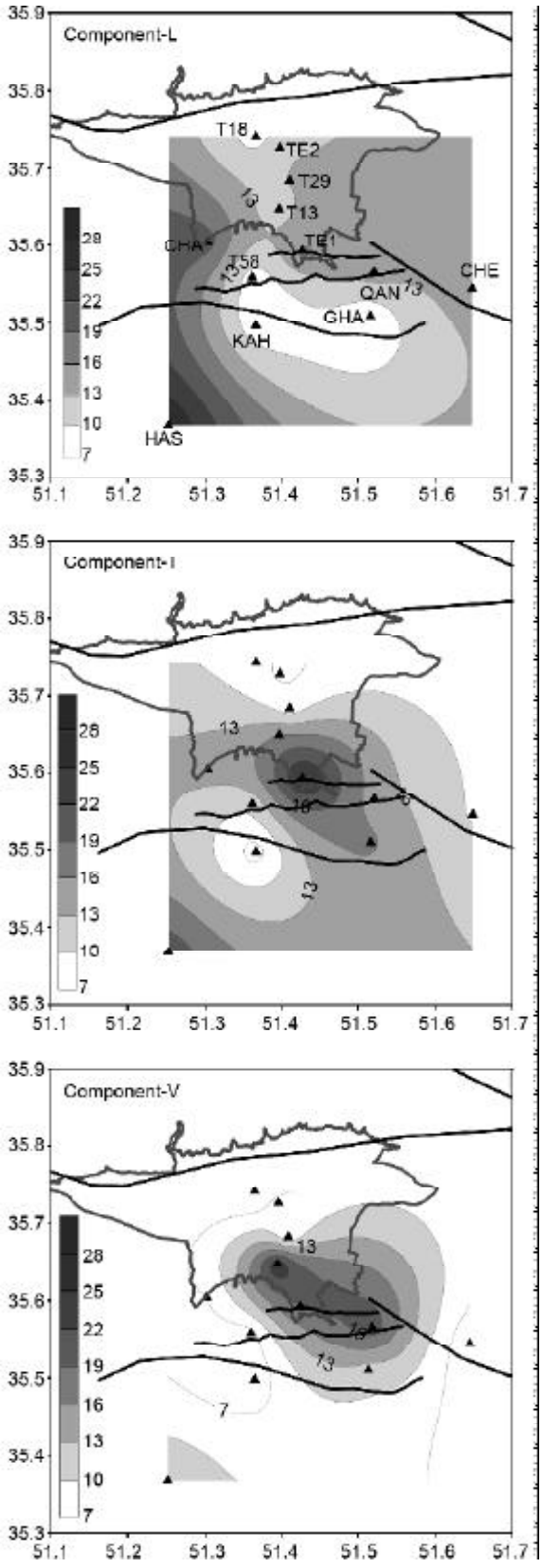

Figure 3. Isoacceleration map for two horizontal components and vertical component. Acceleration counters are in cm/sec^2.

We first investigate the *SH*-wave acceleration time histories, derived from these induced ground motion time histories and then, a non-linear least square analysis of the spectral components of this derived *SH*-wave data was performed to estimate causative fault parameters. We derived accelerograms transverse to the azimuth directions from the recorded acceleration data in the following way [14-15]. The estimated earthquake epicenters reported by different agencies were considered and the back azimuths to the epicenters from *BHRC* stations were calculated and the horizontal component accelerograms were suitably rotated. These transverse accelerograms can be reliably assumed to be good representations of the corresponding *SH*-wave accelerograms of this event. For estimation of causative fault plane parameters, we have considered only five out of 12 stations. These stations are Tehran-1, Tehran-13, Ghaniabad, Hassan Abad, and Chahardangeh.

4. Method

4.1. Estimation of Q_S

In this study, the quality factor of *S*-waves, Q_s is estimated by applying the extended coda normalization method [16]. It exploits the proportionality among the spectral amplitudes of coda, and *S*-waves for the estimation of Q_s. This method assumes that earthquakes occurring at different locations within a small magnitude range have the same spectral ratio of *S*-wave radiation within a narrow frequency range. For spherically outgoing *S*-wave of frequency *f* in a uniform velocity structure, the spectral amplitude at a travel distance *r* goes roughly as:

$$U^{S-Direct}(f,r) \propto \sqrt{W_i^S(f)}N_j^S(f)e^{-\pi frQ_S^{-1}/V_S}/r \qquad (1)$$

Where, $N_j^s(f)$ is the site amplification factor, W_i^S is the *S*-wave source energy, V_S is the *S*-wave velocity. Coda waves provide a reliable way to isolate and quantify seismic propagation effects. Based on the single scattering model [17], we may write the average coda amplitude at a long lapse time t_c from the origin time at central frequency *f* as a product of the source, propagation and site amplification as:

$$U^{S-Coda}(f,t_c) \propto \sqrt{g_o(f)W_i^s(f)}N_j^s(f)e^{-Q_c^{-1}\pi ft_c}/t_c \quad (2)$$

It is supposed that $g_o(f)$ (scattering coefficient) is constant. Aki [18] proposed a correction for source size and site amplification by normalizing direct *S*-wave amplitude by *S*-coda amplitude. Taking the logarithm of the ratio of the product of *r* and the direct *S*-wave amplitude to the averaged coda amplitude, where the common site amplification and source terms cancel, we get:

$$ln[rU^{S-Direct}(f,r)/U^{S-Coda}(f,t_c)] = -(Q_s^{-1}(f)\pi f/V_s)r + Const \qquad (3)$$

Plotting the left-hand side of (3) against *r*, the slope gives the attenuation per travel distance. Applying the least-squares method to plots of the left-hand side of equation (3) against the hypocentral distance, Q_s can be estimated from linear regression lines.

4.2. Non-Linear Least Square Analysis of SH-Wave Spectral Data

It was noted that *SH*-waves were minimally affected by the crustal heterogeneities [19]. Moreover corrections for mode conversion at the free surface for *SH*-waves were not needed and therefore, a full space representation for the earthquake source region could be adopted. The *SH*-wave acceleration spectral data were obtained using a Fast Fourier Transform (*FFT*) along with a Hamming-Tukey window to reduce the effect of data truncation. The corresponding amplitude spectra of *SH*-wave displacement data were first corrected for hypocentral distance in order to bring these to the same reference level. With a further correction for free surface effect, the resulting data set could be approximately treated as if recorded in a full space [15].

We now best-fit Brune ω^{-2} spectra, in the manner outlined below, to these corrected observed *SH*-wave displacement spectral data at the various stations. The mathematical expression was used [20-21]:

$$D(f,R) = W_oGS(R)exp(-\pi ft/Q_S)/[1+(f,f_c)^2] \quad (4)$$

In this mathematical expression, $D(f,R)$ is the displacement spectrum, W_o is long period spectral level, *f* is frequency in *Hz*, *t* is travel time, Q_S is the quality factor of *S*-waves, *R* is the source-receiver distance and $GS(R)$ accommodates for geometrical spreading. $GS(R) = R^{-1}$ for $R \le R_y$ and $GS(R) = (RR_y)^{-0.5}$ for $R > R_y$ [22]. R_y, which was taken as

90*km*, may be taken twice of the crust thickness for this region [22].

The other two parameters viz. the zero-frequency spectral level (W_o) and corner frequency (f_c) were next estimated [23-24]. Stable estimates of W_o and f_c can be obtained from recorded data using estimates of the integral of the square of the ground velocity (J) and the cumulative displacement squared (K). The following formulations for J and K have been proposed [23-24]:

$$J = 2\int_0^{\infty} |\omega D(\omega, R)|^2 d\omega = \frac{2}{3}[W_o \omega_1]^2 f_1 + 2\int_{f1}^{f2} |\omega D(\omega, R)|^2 d\omega + 2|\omega_2 D(\omega_2, R)|^2 f_2 \quad (5)$$

$$K = 2\int_0^{\infty} |D(\omega, R)|^2 d\omega = 2|D(\omega_1, R)|^2 f_1 + 2\int_{f1}^{f2} |\omega D(\omega, R)|^2 d\omega + \frac{2}{3}[D(\omega_2, R)]^2 f_2 \quad (6)$$

where $\omega = 2\pi f$. Here $D(\omega, R)$, the far field displacement in the frequency domain is assumed to have a constant amplitude for $f < f_1 (\omega_1 = 2\pi f_1)$ and a ω^{-2} fall-off for $f > f_2$ ($\omega_2 = 2\pi f_2$). Then W_0 and f_c are given by the formulations [24]:

$$W_o = (4K^3/J)^{1/4} \text{ and } f_c = (J/4\pi^2 K)^{1/2} \quad (7)$$

Our acceleration data has been filtered with a Butterworth filter of order 4 in the frequency range 0.20 to 25.0*Hz*. The derived *SH*-wave spectral data were used from each of the eight stations in the limited frequency band (0.20-10.0*Hz*), so that f_1 and f_2 were taken as 0.2 and 10.0*Hz* respectively, and estimated J and K, see Eqs. (5) and (6), and thereby W_0 and f_c, see Eq. (7).

In the formulation of W_o, see Eq. (7), the order of J and K were different. Possibly because of this, our estimated W_o values were quite unstable and always depended on the estimated corner frequency f_c. To overcome this difficulty, it was noted from the available accelerograms, $D(\omega, r)$ values corresponding to eight to sixteen arbitrarily chosen frequencies less than the earlier estimated corner frequency (f_c), calculated the mean of these $D(\omega, r)$ values and then estimated W_o using Eq. (4). In this manner, we estimated appropriate values of the three parameters (W_o and f_c) for the best-fit Brune's spectrum, see Figure (4), corresponding to the corrected displacement spectral data available at the selected stations for main shock [14-15].

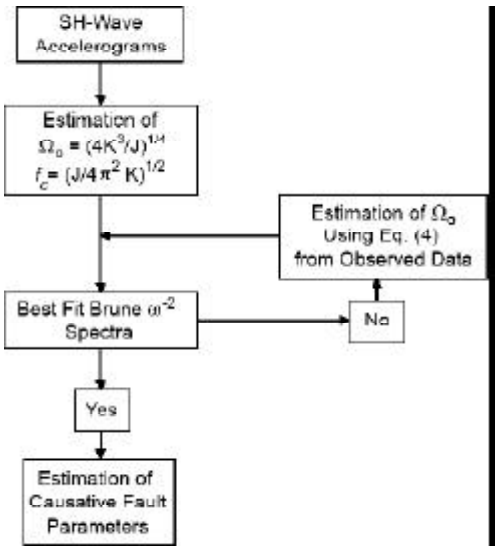

Figure 4. Flowchart of estimation of causative fault parameters.

Then, the causative fault parameters (strike, dip, slip) were estimated by following a non-linear least square analysis of the displacement spectral data already reported in literature [14-15]. In this scheme the non-linear least square error function is defined as:

$$E(strike,\ dip,\ rake) = \sum_i (A_{oi} - A_{ti})^2 \quad (8)$$

where A_{oi} and A_{ti} denote the observed and theoretical estimates of the spectral *SH*-wave amplitudes of displacement at the i^{th} station. A_{oi} values can be read directly from the observed *SH*-wave spectra; the corresponding A_{ti} can be obtained from the formula for radiation pattern for far field *SH*-waves from a point double couple source [25]. This formula depends on the fault orientation parameters (i.e. fault strike, dip and rake), source take off angle and station azimuth. The values of A_{oi} and A_{ti} were used at the corner frequency f_c which were estimated above from the best-fit Brune spectrum analysis. However, it is worthy of note here that, since the fault plane solution is preserved over the entire spectrum, any of its section could have been used for estimating the fault plane solution. E (strike, dip, rake) was optimized in the non-linear least square sense using a grid search procedure to simultaneously

obtain approximate estimates for the strike, dip and rake of the causative fault.

4.3. H/V Method for Strong Motion Records

H/V ratio that is called receiver function [26-28] and Quasi-Transfer Spectra (*QTS*) technique [29] is a tool to estimate the effect of surface geology or surface soil/sediment layer without needing other geological information. In order to estimate the spectral seismic response function for a specific single three component station without hard rock site reference station, the spectral ratios of horizontal to vertical components (*H/V* ratio) of the whole signal including *P* and *S* wave parts of the strong motion records was calculated and analyzed [27]. The calculation procedure included:

i) Selection of a processing time window (*S* and *S*-coda waves [29] and *P*-*S* windows [27];
ii) Calculation of amplitude spectra followed by *H/V* spectral ratios and their smoothing in a frequency window, and
iii) Calculation of the average *H/V* ratio (over both horizontal components). The formulation used for the computation of horizontal to vertical spectral ratio is as follow [28]:

$$SR_{hv}=\frac{\sqrt{\frac{1}{2}\left(\frac{S_{H1}{}^2}{T_{H1}}+\frac{S_{H2}{}^2}{T_{H2}}\right)}}{\frac{S_V(f)}{\sqrt{T_V}}} \qquad (9)$$

in which T_{H1}, T_{H2} are the horizontal components and T_V is the vertical component signal durations. Since the same time window is used for each three component record, then $T_{H1}=T_{H2}=T_V$ and this equation will simplify as:

$$SR_{hv}=\frac{\sqrt{\frac{1}{2}\left(S_{H1}(f)^2+S_{H2}(f)^2\right)}}{S_V(f)} \qquad (10)$$

In this study, this ratio is considered, where the signal to noise ratio is greater than or equal 3. The signal to noise ratio is computed by using Eq. (11):

$$R_{sn}=\frac{S(f)/\sqrt{t_s}}{N(f)/\sqrt{t_n}} \qquad (11)$$

where t_s and t_n are signal and noise windows duration. In the computation of this ratio the smoothing method is used [30].

5. Results and Discussions

The accelerograms have been filtered at five different central frequencies of 1.5 (1-2*Hz*), 3 (2-4*Hz*), 6 (4-8*Hz*), 12 (8-16*Hz*) and 24*Hz* (16-32*Hz*) using a four-pole Butterworth band-pass filter. The *S*-wave analysis was based on the *SH*-waves because these are minimally affected by crustal heterogeneity, see Figure (5a). We plotted the arithmetic mean Q_s in five frequency bands at whole stations with the standard deviations represented by error bars, see Figure (5b). The frequency dependent relationship for *S*-waves was in the form of $Q_s(f)=(92.0\pm16.0)\,f^{(0.98\pm0.15)}$. The estimated frequency dependent relationship was closed to relation given for central Alborz as $Q_s(f)=90\,f^{0.74}$ [31]. This shows that the attenuation characteristics in the Tehran are the same as active regions of the world, while seismically active regions show low Q_s values. Q_o (Q at 1*Hz*) represents the level of

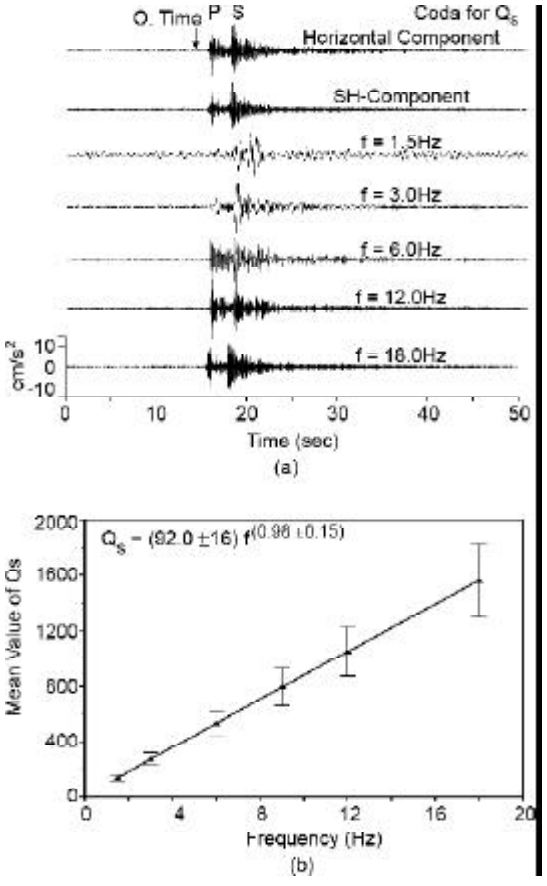

Figure 5. (a) The acceleration record, followed by SH component and filtered records, (b) plot of mean value of Q_s.

medium heterogeneities. It has been found that the regions of high tectonic activity are characterized by low Q_o compared to stable region [32]. The Q_o map has been shown in Figure (6), which shows Q_o is decreasing as we move towards the north within the Tehran city. This shows that attenuation is faster as moving towards north within Tehran.

The *H/V* ratio has been estimated for all five records, which have been used for estimation of causative fault parameters, see Figure (7) and Table (2). The main advantage of this technique is its independence from the reference site [33]. The validity of the results of *H/V* method strongly depends on how well the time processing windows correspond to single, non-interfering, phases. In

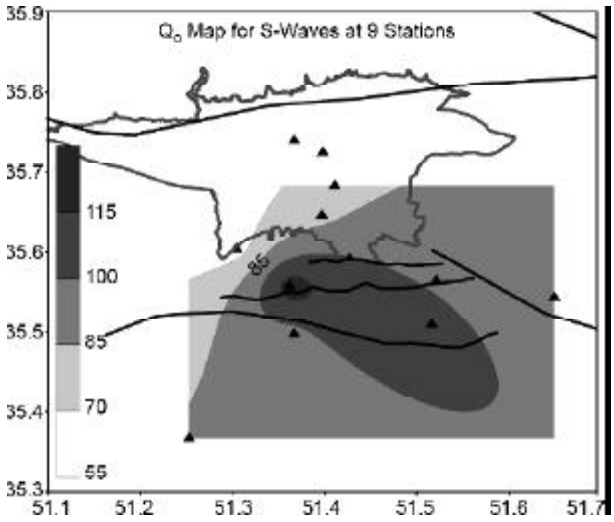

Figure 6. Q_o map at frequency of 1Hz.

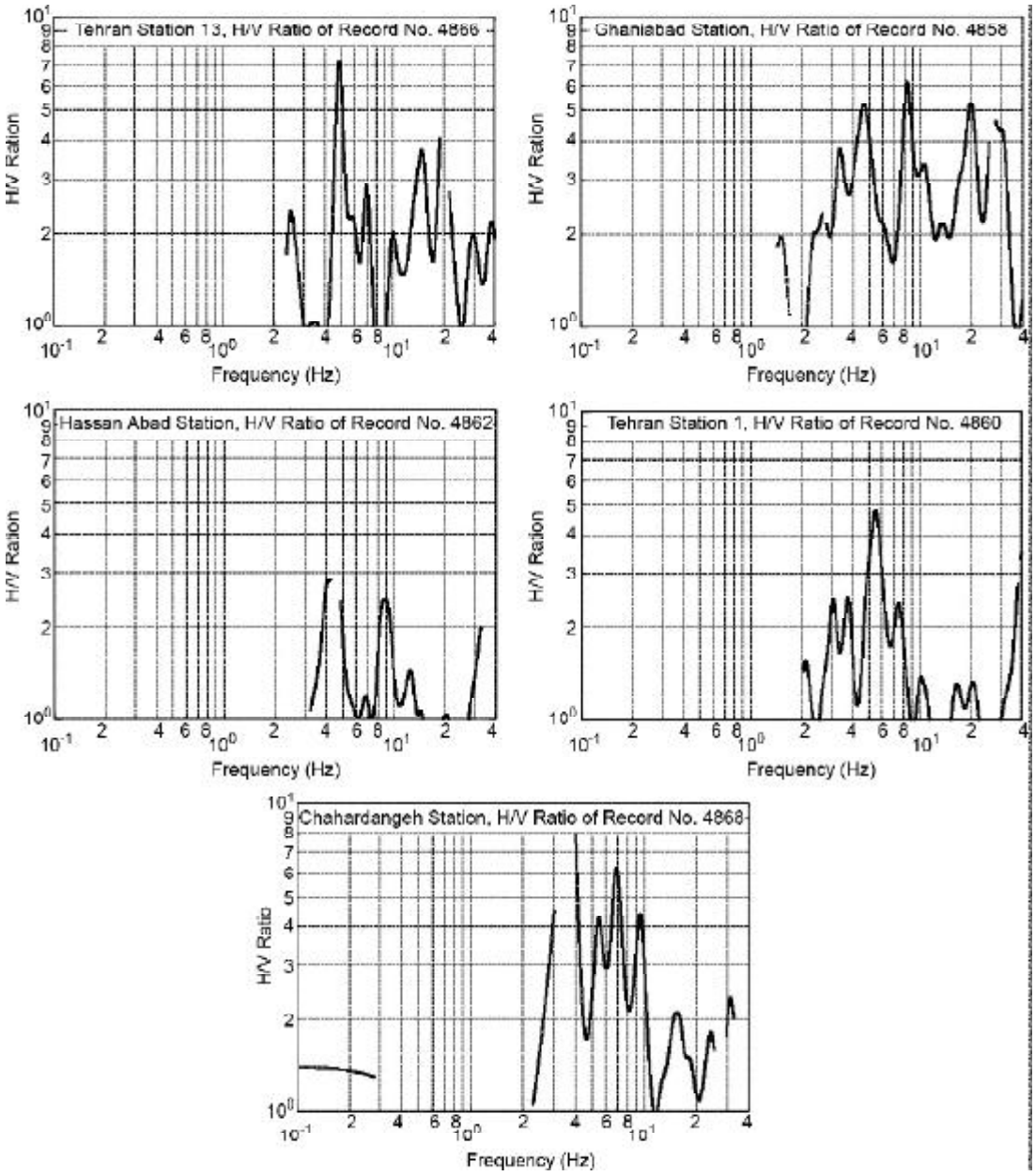

Figure 7. The H/V ratio at Tehran-1, Tehran-13, Ghaniabad, Hassan Abad and Chahardangeh stations.

fact *H/V* does not have any physical meaning when interfering waves are considered [33-34]. Nakamura's method can reveal the fundamental resonant frequency of a site but that is usually not able to give the correct amplification level [34]. Since a reference site was not available to estimate the frequency bands of significant amplification, the amplification characteristics described here in Figure (7) are only relative. But note the significant amplification at each station is in the range of approximately 4-7*Hz*, which is more than the estimated corner frequency of 1.3*Hz* for this event.

Despite this drawback, the overall comparison of the observed and simulated displacement spectra was considered, see Figure (8), as a fair support for the reliability of our near field estimates of W_o and

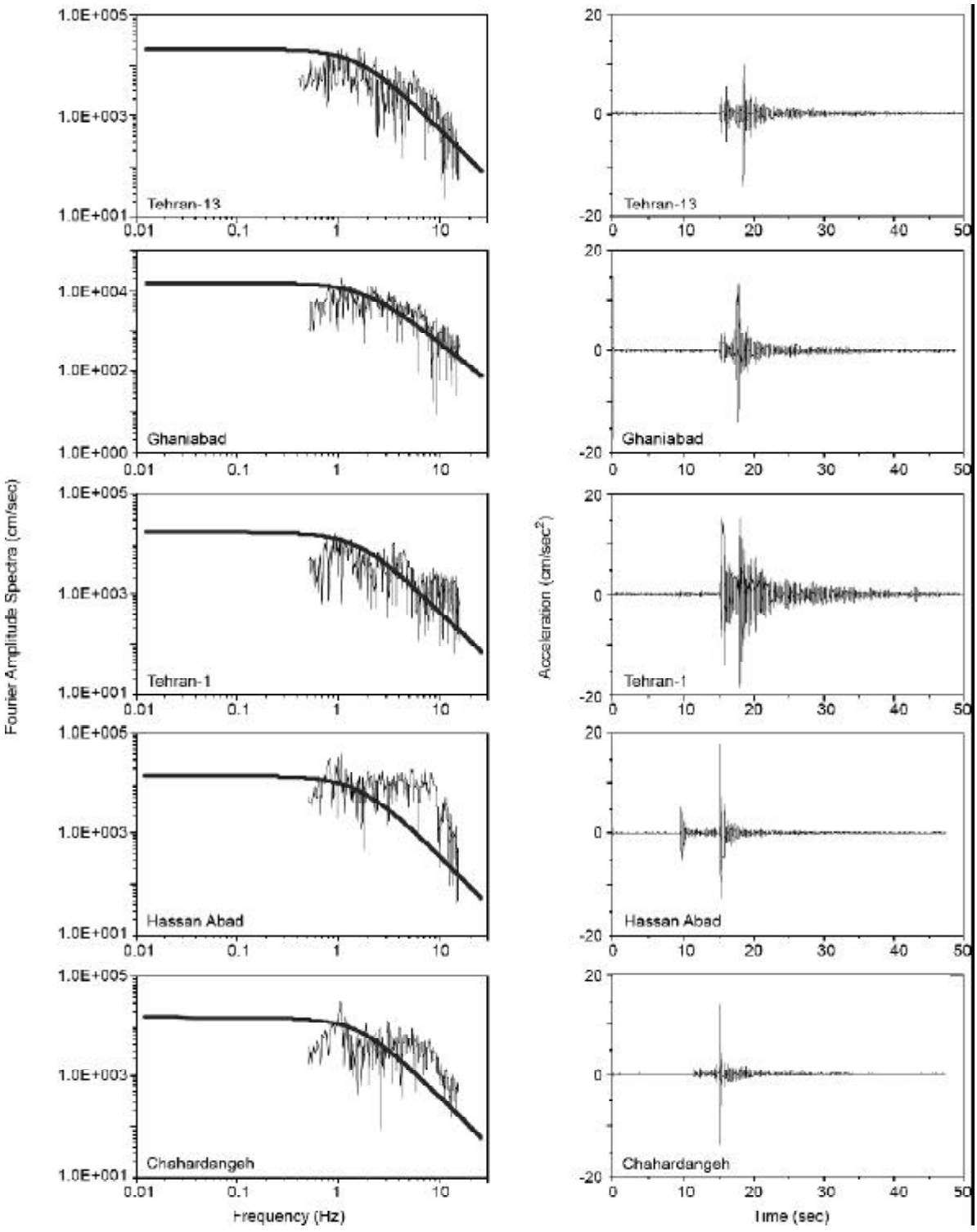

Figure 8. The SH waves (right) and observed and best fit displacement Brune spectrum (left).

Table 2. The dominant frequencies and H/V ratios of recorded accelerograms.

Station	Dominant Fr. (Hz)	H/V Ratio
Ghaniabad	4.5	5
Tehran-1	5.5	5
Hassan Abad	4.5	<3
Tehran-13	5	7
Chahardangeh	7	6

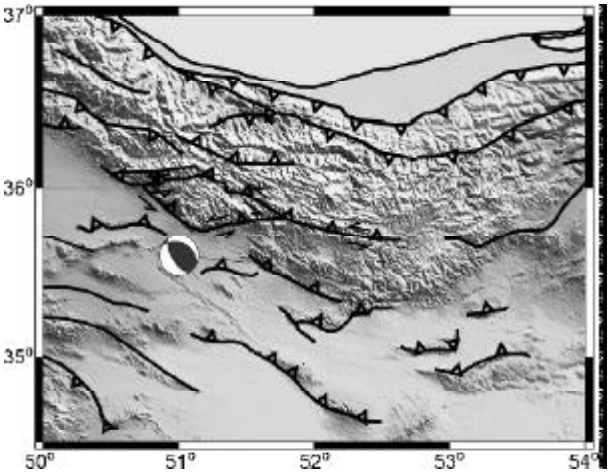

Figure 9. Focal mechanism of Ray-Tehran earthquake from analysis of SH-waves near field data.

f_c. Of course the difficulty to determine the non-linearly related uniquely and reliably W_o and f_c (as in Eq. (4)) from a spectral analysis of band-limited near field data is well recognized. But it is also worthy of mention here that our near field estimates of f_c for the event viz.1.3*Hz* compare well with f_c value of similar sized earthquakes reported from other far field, broadband data analysis [35].

The *SH*-wave accelerograms from the five stations Tehran-1, Tehran-13, Ghaniabad, Hassan Abad and Chahardangeh provide some insight into the characteristics of propagation of the causative rupture of the main event, see Figure (8). The accelerograms at Tehran-1, Tehran-13, and Ghaniabad lying to the northwest of the *TDMMO* [13] located hypocentre, exhibited front-loaded shear wave energy release suggesting that these stations are located in the direction of rupture propagation. It was further noted that the accelerogram at Hassan Abad is more spread out than the accelerogram at Tehran-1, Tehran-13, and Ghaniabad possibly implying that the rupture propagated toward northwest.

To estimate the causative fault parameters, *IIEES*, *IGTU* and *TDMMO* [13] locations have been considered. Our near field estimates of the strike, dip and rake of causative fault are given in Table (3). The fault plane solution suggests reverse faulting with left lateral strike slip motion, see Figure (9). The estimated strike, dip and rake for the causative fault are 292°, 36° and 59°, respectively. The total standard error of estimate is 0.16 by considering *TDMMO* location, while these estimates for *IIEES* and *IGTU* locations are 0.26 and 0.24, respectively. The direction of the estimated strike is consistent with the direction of isoacceleration maps, see Figure (3), as well as the strike of Eyvanaki fault, see Figure (2).

7. Conclusions

The following are the conclusions of this study:

- Our method of analysis of near field, band limited data has also provided fairly reliable, worthwhile results. It thus appears worthy for analyzing similar not-very-good quality, near field data from other such small seismic events.
- The knowledge of seismic wave attenuation is very important for Tehran for quantitative prediction of strong ground motion in the assessment of earthquake hazard. Q_s has been estimated for Ray-Tehran using the extended coda normalization method. Based on the analysis, the frequency dependent relations in the form of $Q_s = 92.0 f^{0.98}$ were found. These results indicated that the Q_s values in this region were some of the highest in the world. The high Q_s values corresponded to those of the seismically active area in the world.
- Near field estimates of the strike, dip and rake of the causative faults of the 2009 Ray-Tehran earthquake were 292°, 36°, and 59°, respectively.
- Our estimated fault plane solutions suggested a

Table 3. Causative fault parameters for the 2009 earthquake.

Date	Standard Error of Estimate	Fault Plane			Auxiliary Plane			P Axis		T Axis	
		Strike	Dip	Rake	Strike	Dip	Rake	P-Az	P-Dip	T-Az	T-Dip
22/10/2009	0.16	292	36	59	149	60	111	224	13	101	68

reverse faulting mechanism with minor left lateral strike slip component. The estimated strike was consistent with the direction of isoacceleration map and Eyvanaki fault.

Acknowledgments

The authors are thankful to International Institute of Earthquake Engineering and Seismology (*IIEES*) and Building and Housing Research Center (*BHRC*) for providing the required data for this research work. We are also thankful to anonymous reviewers whose suggestions helped significantly in improving the paper.

References

1. Sengor, A.M.C., Altiner, D., Cin, A., Ustaomer, T., and Hsu, K.J. (1988). "Origin and Assembly of the Tehyside Orogenic Collage at the Expense of Gondwana Land", In: Audley-Charles, M.G., Hallam, A. (Eds.), Gondwana and Thetys.

2. Jackson, J., Priestley, K., Allen, M., and Berberian, M. (2000). "Active Tectonics of the South Caspian Basin", *Geophys. J. Int.*, **148**, 214-245.

3. Allen, M.B., Ghassemi, M.R., Sharabi, M., and Qoraishi, M. (2003). "Accomodation of Late Cenozoic Oblique Shortening in the Alborz Range, Northern Iran", *J. Struct. Geol.*, **25**, 659-672.

4. Vernant, Ph., Nilfroushan, F., Chery, J., Bayer, R., Djamour, Y., Masson, F., Ritz, J.F., Sedighi, M., and Tavakoli, F. (2004). "Deciphering Oblique Shortening of Central Alborz in Iran Using Geodetic Data", Earth and Planetary Science Letters, **223**, 177-185.

5. Abbassi, M.R. and Farbod, Y. (2009). "Faulting and Folding in Quaternary Deposits of Tehran's Piedmont (Iran)", *Journal of Asian Earth Sciences*, **34**, 522-531

6. Berberian, M. (1983). "The Southern Caspian: a Compressional Depression Floored by a Trapped, Modified Oceanic Crust", *Can. J. Earth Sci.*, **20**, 163-183.

7. Ashtary, M., Hatzfeld, D., and Kamalian, N. (2005). "Microseismicity in the Region of Tehran", *Tectonophysics*, **395**, 193-208.

8. Trifonov, V.G., Hessami, K.T., and Jamali, F. (1996). "West-Trending Oblique Sinitral-Reverse Fault System in Northern Iran", IIEES Special Pub., **75**, Tehran, Iran.

9. Ritz, J.-F., Balescu, S., Soleymani, S., Abbassi, M., Nazari, H.,Feghhi, K., Shabanian, E., Tabassi, H., Farbod, Y., Lamothe, M., Michelot, J.-L., Massault, M., Che´ry, J., and Vernant, P. (2003). "Determining the Long-Term Slip Rate Along the Mosha Fault, Central Alborz, Iran", Implications in Terms of Seismic Activity, S.E.E. 4 Meeting, Tehran.

10. Berberian, M. and Yeats, R.S. (1999). "Patterns of Historical Earthquake Rupture in the Iranian Plateau", Bulletin of the Seismological Society of America, **89**, 120-139.

11. Ambraseys, N.N. and Melville, C.P. (1982). "A History of Persian Earthquakes", Cambridge University Press, London, 219p.

12. Hamzehloo, H., Vaccari, F., and Panza, G.G. (2007). "Towards a Reliable Seismic Microzonation in Tehran, Iran", *Engineering Geology*, **93**, 1-16.

13. Yaminifard, Personal Communication.

14. Hamzehloo, H. (2005). "Determination of Causative Fault Parameters for some Recent Iranian Earthquake Using Near Field Sh-wave Data", *Journal of Asian Earth Sciences*, **25**, 621-628.

15. Hamzehloo, H., Rahimi, H., Sarkar, I., Mahood, M., Mirzaei Alavijeh, H., and Farzanegan, E. (2009). "Modeling the Strong Ground Motion and Rupture Characteristics of the March 31, 2006, Darb-e-Astane Earthquake, Iran, Using a Hybrid of Near-Field SH-Wave and Empirical Green's Function Method", *J. of Seismology*, DOI10.1007/s10950-009-9159-x.

16. Yoshimoto, K., Sato, H., and Ohtake, M. (1993). Frequency-Dependent Attenuation of P and S Waves in the Kanto Area, Japan, Based on the Codanormalization Method", *Geophys. J. Int.*, **114**, 165-174.

17. Aki, K. and Chouet, B. (1975). "Origin of Coda Waves: Source, Attenuation and Scattering Effects", *J. Geophys. Res.*, **80**, 3322-3342.

18. Aki, K. (1980). "Attenuation of Shear-Waves in the Lithosphere for Frequencies from 0.05 to 25Hz", *Phys. Earth Planet. Inter.*, **21**, 50-60.

19. Haskell, N.A. (1960). "Crustal Reflection of Plane SH Waves", *J. of Geophysical Research*, **65**, 4147-4150.

20. Brune, J.N. (1970). "Tectonic Stress and Spectra of Shear Waves from Earthquakes", *Journal Geophys. Res.*, **75**, 4997-5009.

21. Brune, J.N. (1971). Correction", *J. Geophys. Res.*, **76**, 5002.

22. Herrmann, R. B. and Kijko, A. (1983). "Modelling Some Empirical Vertical Component Lg Relations", *Bull. Seismo. Soc. Am.*, **73**, 157-171.

23. Andrews, D.J. (1986). "Objective Determination of Source Parameters and Similarity of Earthquakes of Different Size", In: Das, S., Boatwright, J., and Scholz, C.H. (Eds), Earthquake source Mechanics, Maurice Ewing, **6**, Geophys. Monogr., **37**, Amer. Geophys. Union, Washington, DC, 259-268.

24. Snoke, J.A. (1987). "Stable Determination of (Brune) Stress Drops", Bulletin Seismological Society of America, **77**, 530-538.

25. Aki, K. and Richards, P.G. (1980). "Quantitative Seismology: Theory and Methods", **1**, W.H. Freeman and Co., San Francisco.

26. Zare, M. (1999). "Contribution à L'étude des Mouvements Forts en Iran: du Catalogue Aux Lois D'Atténuation", PhD Thesis, Université Joseph Fourier, Grenoble, France.

27. Theodulidis, N.P. and Bard, P.Y. (1995). "Horizontal to Vertical Spectral Ratio and Geological Conditions: An Analysis of Strong Motion Data from Greece and Taiwan (SMART-1)", *Soil Dynamics and Earthquake Engineering*, **14**, 177-197.

28. Sardinal, V.H.R. and Midorikawa, S. (2004). "Site Classification Based on Spectral Amplification Patterns For Microtremor H/V Ratios", *13th World Conference on Earthquake Engineering Vancouver*, B.C., Canada, Paper No. 1770.

29. Nakamura, Y. (1989). "A Method for Dynamic Characteristics Estimation of Subsurface Using Microtremor on the Ground Surface", QR of RTRI, **30**(1), 25-33.

30. Konno, K. and Ohmachi, T. (1998). "Ground-Motion Characteristic Estimated from Spectral Ratio between Horizontal and Vertical Components of Microtremor", Bull. Seism. Soc. Am., **88**, 228 -241.

31. Ghasemi, H., Kamalian, N., Hamzehloo, H., and Beitollahi, A. (2005). "Attenuation of Shear-Waves in the Alborz Region for Frequencies from 1 to 32Hz, Using Near Field Accelerograms Obtained During Baladeh-Kojour Earthquake", *Journal Earth and Space Physics*, **31**(1), 103-112.

32. Paul, A., Gupta, S.C., and Pant, C.C. (2003). "Coda Q Estimates for Kuman Himalaya", *Earth Planet. Sci.*, **112**, 569-576.

33. Panza, G.F., Romanelli, F., and Vaccari, F. (2001). Seismic Wave Propagation in Laterally Heterogeneous Anelastic Media: Theory and Applications to Seismic Zonation", *Advances in Geophysics*, **43**, 1-95.

34. Paskaleva, I., Dimova, S., Panza, G.F., and Vaccari, F. (2007). "An Earthquake Scenario for the Microzonation of Sofia and the Vulnerability of Structures Designed by Use of the Eurocodes", *Soil Dynamics and Earthquake Engineering*, **27**, 1028-1041.

35. Singh, S.K., Mohanty, W.K., Bansal, B.K., and Roonwal, G.S. (2002). "Ground Motion in Delhi from Future Large/Great Earthquakes in the Central Seismic Gap of the Himalayan Arc", Bull. Seism. Soc. Am., **92**, 555- 569.